# Critical structure in the density of states from non-atom-centered Wannier functions

G. H. O. Daalderop
*Philips Research Laboratories, P.O. Box 80 000, NL-5600 JA Eindhoven, The Netherlands*

M. H. Boon
*Department of Theoretical Physics, University of Nijmegen, NL-6525 ED Nijmegen, The Netherlands*

F. M. Mueller
*Center for Materials Science, Los Alamos National Laboratory, Los Alamos, New Mexico 87545*
(Received 22 November 1989)

It is shown that the highest and most prominent peak in the density of states of fcc Ni at the top end of the $d$ region can be derived from antibonding Wannier functions of $\Gamma'_{12}$ ($h$ symmetry) centered at $(\frac{1}{2},\frac{1}{2},\frac{1}{2})$ in units of the lattice constant. It is suggested that there is a close relationship between high peaks in the density of states of other systems and similar compact bases consisting of non-atom-centered localized functions.

## I. INTRODUCTION

Many properties of metals can be derived from an understanding of the electronic density of states, $N(E_F)$, in the vicinity of the Fermi level $E_F$. In general those materials which exhibit narrow and high peak structures in the density of states near $E_F$ also exhibit unusual and interesting superconducting or magnetic behavior. A concomitant problem is that materials with very high $N(E_F)$ seem to be rare, probably because such materials are inherently unstable.

The root causes for the existence of peaks in the density of states were investigated topologically in the mid 1950s and stem from Van Hove critical points or singularities,[1] i.e., places in the Brillouin zone (BZ), $\mathbf{k}$, where

$$\nabla[\varepsilon_n(\mathbf{k})]=0 , \tag{1}$$

which characterize the structure in $N(E)$. Peaks in the density of states arise from a confluence in energy of critical points with lower $M_1$ and upper $M_2$ character, i.e., critical points where the local mass tensor has one or two negative mass components. Around these critical points the local electronic band structure is hyperboloidal; a plot of local constant-energy contours shows first the passage from a hyperbola of two sheets to a hyperbola of one sheet and then the reverse behavior, as the energy is increased. Twice in this procedure the constant-energy contours will pass through the case of an intersecting cone, whose surface area is a relative maximum. Because of the change in the local topology, such behavior leads immediately to discontinuities in the derivative of the density of states and the two critical points together make one single peak if the critical points are close in energy. There is thus a close relationship of both the energy surface area and the energy-band dispersion to peaks in the density of states:

$$N(E)=\frac{2\Omega}{(2\pi)^3}\sum_n \int d\mathbf{k}\,\delta(\varepsilon_n(\mathbf{k})-E)$$
$$=\frac{2\Omega}{(2\pi)^3}\sum_n \int \frac{dS}{|\nabla\varepsilon_n(\mathbf{k})|} , \tag{2}$$

where $n$ is a band index, $\mathbf{k}$ is a point in the Brillouin zone, and $\varepsilon_n(\mathbf{k})$ is the energy surface $E=\varepsilon_n(\mathbf{k})$. The fundamental structure in the density of states of any material is fully understandable on the basis of such Van Hove singularities (ignoring for the moment the complications of fluted and singular critical points[2]).

Rather less attention has been paid to the nature of the local behavior (in $\mathbf{k}$) of the electronic wave function which accompanies a Van Hove singularity. Since a Van Hove singularity is, by definition, a place in $\mathbf{k}$ where the energy band itself is stationary, what is the consequence for the $\mathbf{k}$ dependence of the wave function? Conversely is it possible to make useful statements about the nature of wave functions at critical points which would help to understand density-of-states peaks in interesting materials? It is the purpose of the present work to investigate the question of the relationship of the wave function to density-of-states structure, which we believe has not been much raised or considered before. Since we wished to treat a concrete, simple, and well-studied example, we will focus in much of what follows on the narrow peak in the density of states exhibited in nickel near the top of the $3d$ region; we expect, however, that most of our arguments will be of more general applicability and validity.

The plan of the paper is as follows. In Sec. II we will consider the insights that $\mathbf{k}\cdot\mathbf{p}$ perturbation theory brings to the critical structure of Ni in the selected energy region. In Sec. III we will introduce a non-atom-centered Wannier function (of $h$ symmetry) to describe and generate the band structure in the neighborhood of the critical point. In Sec. IV we will formulate a Slater-Koster-like model Hamiltonian based on these Wannier func-

 

tions [centered at the set of Wyckoff points equivalent to $a(\frac{1}{2},\frac{1}{2},\frac{1}{2})$, where $a$ is the fcc lattice constant], and compare the band structure based on this model with the results of standard augmented-spherical-wave (ASW) calculations. In Sec. V we summarize our work and draw our conclusions.

## II. DEVELOPMENT OF k·p HAMILTONIAN

One of the most prominent features in the density of states of any material with which we are familiar is the large peak in the density of states associated with the top end of the $d$ band of the fcc materials: Ni, Pd, and Pt. In Fig. 1 we show a typical fcc density of states, that of nickel.[3] The peak of interest is dominantly associated with the electronic structure of band 5 whose partial density of states is shown in Fig. 1 as the dashed curve and whose area is hatched. Although Fig. 1 is rich in structure, the number of critical points is modest: there are 27 critical points or about 5.4 per band. Since the minimum possible number is four critical points per band, there is not a very large increase over the minimal possible set. This says that the electronic structure of Ni is not complicated or alternatively that the far distant (in a Wannier or tight-binding sense) neighbor interactions are weak (if they were strong, one consequence would be a multiplicity of maxima and minima, and a great increase in the number of critical points beyond the number of 4).

In Fig. 2 the corresponding electronic band structure of nickel along the high-symmetry directions of the BZ is shown.[3] The strongest feature of band 5 is the flat line from the $X_5$ doublet to $W_{1'}$ along $Z_2$. This means that in this region the mass component along the $Z$ line ($X-W$) is very large, about $-54.5$ electron masses for the bands of Fig. 2. Along line $S$ ($U-X$) and line $\Lambda$ ($\Gamma-L$) the masses are about $-0.8$ and $-2.5$, 1–2 orders of magnitude smaller than along line $Z$. There is very little dispersion along line $Z$, revealing the cylindrical or two-dimensional nature of the electronic structure in this region. This same structure produces the "jungle gym" Fermi surface of band 5 in Pd and Pt found to have heavy mass.[4] Because the topology of the electronic structure has been altered by the high mass along line $Z$ from that of a three- to two-dimensional type in this region, there is a corresponding change in the Van Hove structure. As is well known, a two-dimensional maximum in the energy bands generates a jump discontinuity in the density of states, observable at the top end of the band-5 partial density of states in Fig. 1. The 5-mRy-wide peak in Fig. 1 around 0.75 Ry is, however, *not* to be associated with the top end band-5 structure in general and the two-dimensional structure around line $Z$ in particular.

From which regions, then, are we to derive this rather large peak exhibited in Fig. 1? Although the integrated volume of the peak is 22% of the volume of the BZ or 0.44 of an electron, the sharp and simple kinks of the density of states with smooth behavior in between strongly suggest that there are two and only two types of critical singularities in this peak, necessarily of type $M_1$ and $M_2$ if we assume them to be analytic. Based on the energy of the $M_2$ critical point, one would like to make it coincident with the high-symmetry point $L$. If we examine closely the electronic structure for band 5 shown in Fig. 2 along three orthogonal directions, then we see that along line $\Lambda$ ($\Gamma-L$), line $Q$ ($L-W$), and line $M$ ($L-U$) the mass tensor appears to be triple negative, i.e., $L$ appears to be an $M_3$ *maximum* critical point, which is not reconcilable with the shape of the density of states. The minimum along the line $Q$ is at the correct energy to be the $M_1$ critical point. The simplicity of the structure of Fig. 1 belies any idea of multiple overlays; the peak structure has (or can have) only two closely related critical points. Where are they?

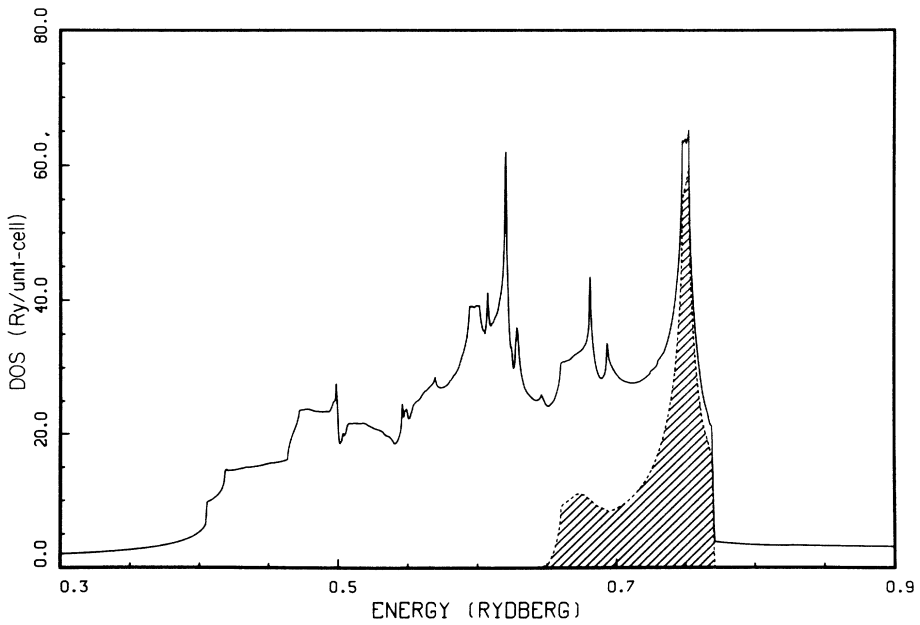


FIG. 1. Density of states of nickel (Ref. 3). The partial density of states for band 5 is shown as the dashed curve.

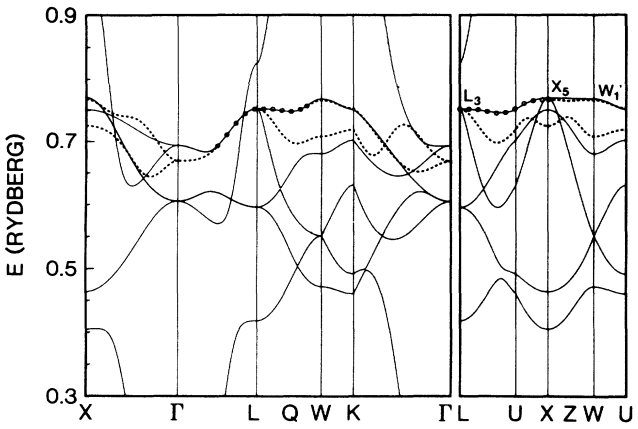


FIG. 2. Electronic band structure of nickel. The solid lines form the spin-down electronic band structure generated by means of the ASW method. The dashed lines are the bands of a 2×2 Hamiltonian, designed to fit band 5 (the uppermost band going through $X_5$ and $L_3$). The range over which the fit was performed is denoted by open circles.

To find the two critical points, we wrote a computer program which searched for the zeros of the gradients of all energy bands.

There were only two fifth-band critical points around 0.75 Ry—one along line $Q$, near $(\pi/a)(0.5,1.0,1.5)$, which was an $M_1$ critical point, and the critical point at $L$ (just visible in Fig. 1 in the full density of states in the region of the peak is a very small $M_3$ singularity due to band 3 at point $X$).

In order to understand the type of singularity at point $L$, at the critical point along line $Q$, and their connectivity, we developed from the Hamiltonian $H$ used for Figs. 1 and 2 a procedure to make $(\mathbf{k}\cdot\mathbf{p})$-like expansions around these critical points. The original band structure was derived by means of the ASW method[3] in which the generalized eigenvalue problem is solved:

$$\sum_{j=s,p,d}[H_{ij}(\mathbf{k})-\epsilon_n(\mathbf{k})S_{ij}(\mathbf{k})]a_j^n(\mathbf{k})=0 \tag{3}$$

where the wave function for band $n$ is given by

$$\Psi_{\mathbf{k}}^n(\mathbf{r})=\sum_{j=s,p,d}a_j^n(\mathbf{k})\Phi_{\mathbf{k}}^j(\mathbf{r})\ , \tag{4}$$

$H$ and $S$ are, respectively, the Hamiltonian and the overlap matrix and $\Phi_{\mathbf{k}}^j$ is a Bloch state. Upon Löwdin orthogonalization[5] the overlap matrix can be transformed away with conservation of the symmetry of the basis leading to the eigenvalue problem:

$$\sum_{j=s,p,d}[H'_{ij}(\mathbf{k})-\epsilon_n(\mathbf{k})\delta_{ij}]b_j^n(\mathbf{k})=0 \tag{5}$$

expressed in an orthonormal basis

$$\Phi_{\mathbf{k}}'^i=\sum_{j=s,p,d}[S_{ij}(\mathbf{k})]^{-1/2}\Phi_{\mathbf{k}}^j \tag{6}$$

and where

$$H'_{ij}(\mathbf{k})=(\Phi_{\mathbf{k}}'^i|\mathcal{H}|\Phi_{\mathbf{k}}'^j)\ . \tag{7}$$

Our procedure will be to fit $H'(\mathbf{k})$ to an expansion in $(\mathbf{k}-\mathbf{k}_0)$, where $\mathbf{k}_0$ is chosen at a point of interest in the zone (i.e., point $L$ or the critical point along line $Q$). This can be achieved in the following way: Let $H'(\mathbf{k}_0)$ be the Hamiltonian at the point $\mathbf{k}_0$, with eigenvalues $\epsilon_n(\mathbf{k}_0)$ and diagonalizing matrix $D(\mathbf{k}_0)$. Let us consider the Hamiltonian at a neighboring point $\mathbf{k}$. We can then define the matrix $\underline{H}''$:

$$H''(\mathbf{k})=D^{\dagger}(\mathbf{k}_0)H'(\mathbf{k})D(\mathbf{k}_0)\ , \tag{8}$$

which is diagonal at $\mathbf{k}_0$. What is being done is to transform the Hamiltonian from the variable $\mathbf{k}$ Bloch basis to the local basis at $\mathbf{k}_0$. Up to terms quadratic in $\mathbf{k}-\mathbf{k}_0$, the matrix elements of $H''(\mathbf{k})$ can be expressed in the form

$$H''_{ij}(\mathbf{k})=\epsilon_i(\mathbf{k}_0)\delta_{ij}+(\mathbf{k}-\mathbf{k}_0)\cdot\mathbf{p}_{ij}+\sum_{\alpha,\beta=x,y,z}(\mathbf{k}-\mathbf{k}_0)_\alpha d_{ij}^{\alpha\beta}(\mathbf{k}-\mathbf{k}_0)_\beta \tag{9}$$

where $\delta_{ij}$ is the Kronecker $\delta$ and the $\mathbf{p}_{ij}$ and $d_{ij}^{\alpha\beta}$ are constants. The Hamiltonian (9) is comparable to one that would be obtained by the usual $\mathbf{k}\cdot\mathbf{p}$ method around $\mathbf{k}=\mathbf{k}_0$, except that the quadratic term is not diagonal (i.e., $d_{ij}^{\alpha\beta}\neq\delta_{ij}\delta_{\alpha\beta}$ due to a different $\mathbf{k}$ dependence of the basis than for $\mathbf{k}\cdot\mathbf{p}$ theory).[6] It can be shown, however, that the constants $p_{ij}^{\alpha}$ *are* the same in the two methods (apart from a factor $\hbar/m$), i.e.,

$$\mathbf{p}_{ij}=\frac{\hbar}{m}\left[\Psi_{\mathbf{k}_0}'^i\left|\frac{\nabla}{i}\right|\Psi_{\mathbf{k}_0}'^j\right]\ , \tag{10}$$

where $\Psi_{\mathbf{k}_0}'^i$ are the eigenfunctions of $H'(\mathbf{k}_0)$ corresponding to the $i$th eigenvalue. To derive the expansion (9) around any point $\mathbf{k}_0$, we applied Eq. (8) to a sequence of Hamiltonians, based on a 3×3×3 cubical grid centered at $\mathbf{k}_0$ augmented with six additional points along the $x$, $y$, and $z$ directions at "(2,0,0)", etc. Hence 33 Hamiltonians were used in all. Each matrix element at the 33 points was then least-squares fit to the 20 three-dimensional polynomials made up of all terms up to and including third order in the components of the vector $(\mathbf{k}-\mathbf{k}_0)$. The errors of the least-squares fit showed that the zeroth-order and linear terms had a numerical error smaller than 1%, the six quadratic terms about 10% (as they involve second derivatives), and the third-order terms were in error by about 50%. They have been included to improve the identification of the matrix elements of $\mathbf{p}$ with the odd coefficients. Incompleteness of the basis set introduces small additional errors in the identification of the linear terms as the optical transition matrix elements (the band wave functions are given by a 9×9 Hamiltonian, and one error for example is due to a lack of $f$-like functions). In Table I we show the coefficients to use in Eq. (9) in atomic units for the lowest six bands for nickel at point $L$.

Remarkable is the fact that at point $L$ the degenerate states for bands 4 and 5 ($L_3$) show a zero coupling to quadratic order to all the lower bands. In fact, the first nonzero coupling terms to these bands is actually quartic. Coupling to band 6 ($L_2'$) begins with linear terms, since such a transition is electric dipole allowed.[7] But this state is relatively far away in energy.

TABLE I. The matrix elements $p_{ij}^{\alpha}$ and $d_{ij}^{\alpha\beta}$ ($\alpha,\beta=x,y,z$) for use in Eq. (9) for nonmagnetic Ni at point $L$ in Rydberg atomic units. The distance between point $\Gamma$ and point $X$ is 0.9437 in these units. The labeling is $L_1$, $L_3^1$, $L_3^2$, $L_3^3$, $L_3^4$, and $L_2'$ for bands 1–6, respectively. The couplings to bands 7–9 are omitted from this list as they are relatively far away in energy.

| | Bands | | | | | |
|---|---|---|---|---|---|---|
| | 1 | 2 | 3 | 4 | 5 | 6 |
| Diagonal terms | | | | | | |
| | 0.4180 | 0.5961 | 0.5961 | 0.7532 | 0.7532 | 0.8257 |
| Matrix elements of $P^x$ | | | | | | |
| 1. | 0.0000 | | | | | |
| 2. | 0.0000 | 0.0000 | | | | |
| 3. | 0.0000 | −0.0001 | 0.0000 | | | |
| 4. | 0.0000 | 0.0000 | 0.0000 | 0.0000 | | |
| 5. | 0.0000 | 0.0000 | 0.0000 | 0.0000 | 0.0000 | |
| 6. | −0.2442 | −0.0586 | 0.1014 | −0.5239 | −0.3025 | 0.0000 |
| Matrix elements of $P^y$ | | | | | | |
| 1. | 0.0000 | | | | | |
| 2. | 0.0000 | 0.0000 | | | | |
| 3. | 0.0000 | 0.0001 | 0.0000 | | | |
| 4. | 0.0000 | 0.0000 | 0.0000 | 0.0000 | | |
| 5. | 0.0000 | 0.0000 | 0.0000 | 0.0000 | 0.0000 | |
| 6. | −0.2442 | −0.0586 | −0.1014 | 0.5239 | −0.3025 | 0.0000 |
| Matrix elements of $P^z$ | | | | | | |
| 1. | 0.0000 | | | | | |
| 2. | 0.0000 | 0.0001 | | | | |
| 3. | 0.0000 | 0.0000 | −0.0001 | | | |
| 4. | 0.0000 | 0.0000 | 0.0000 | 0.0000 | | |
| 5. | 0.0000 | 0.0000 | 0.0000 | 0.0000 | 0.0000 | |
| 6. | −0.2442 | 0.1171 | 0.0000 | 0.0000 | 0.6049 | 0.0000 |
| Matrix elements of $D^{xx}$ | | | | | | |
| 1. | 1.1222 | | | | | |
| 2. | 0.1335 | 0.2533 | | | | |
| 3. | −0.2312 | 0.2385 | −0.0242 | | | |
| 4. | −0.0969 | 0.0494 | 0.0355 | −0.5773 | | |
| 5. | −0.0559 | −0.0920 | −0.0495 | −0.1098 | −0.4507 | |
| 6. | 0.0000 | −0.0001 | 0.0000 | 0.0000 | −0.0001 | 1.4192 |
| Matrix elements of $D^{yy}$ | | | | | | |
| 1. | 1.1222 | | | | | |
| 2. | 0.1335 | 0.2534 | | | | |
| 3. | 0.2312 | −0.2382 | −0.0243 | | | |
| 4. | 0.0969 | −0.0495 | 0.0356 | −0.5772 | | |
| 5. | −0.0559 | −0.0920 | 0.0495 | 0.1099 | −0.4507 | |
| 6. | 0.0000 | 0.0000 | 0.0001 | −0.0001 | 0.0000 | 1.4192 |
| Matrix elements of $D^{zz}$ | | | | | | |
| 1. | 1.1222 | | | | | |
| 2. | −0.2669 | −0.1594 | | | | |
| 3. | 0.0000 | 0.0000 | 0.3886 | | | |
| 4. | 0.0000 | 0.0000 | 0.1213 | −0.3870 | | |
| 5. | 0.1119 | −0.0063 | 0.0000 | 0.0000 | −0.6410 | |
| 6. | 0.0000 | −0.0002 | 0.0001 | −0.0001 | −0.0002 | 1.4192 |
| Matrix elements of $D^{xy}$ | | | | | | |
| 1. | −0.7530 | | | | | |
| 2. | −0.8814 | −0.6233 | | | | |
| 3. | −0.0002 | 0.0011 | 0.7677 | | | |
| 4. | 0.0002 | −0.0003 | −0.2882 | 0.8159 | | |
| 5. | 0.2401 | 0.0573 | 0.0003 | 0.0002 | −0.7927 | |
| 6. | 0.0000 | −0.0001 | −0.0001 | 0.0001 | 0.0000 | −0.6157 |

TABLE I. (*Continued.*)

| | Bands | | | | | |
|---|---|---|---|---|---|---|
| | 1 | 2 | 3 | 4 | 5 | 6 |
| Matrix elements of $D^{yz}$ | | | | | | |
| 1. | −0.7530 | | | | | |
| 2. | 0.4409 | 0.4203 | | | | |
| 3. | −0.7628 | 0.6013 | −0.2759 | | | |
| 4. | −0.2083 | −0.0998 | −0.1149 | −0.3904 | | |
| 5. | −0.1199 | 0.2306 | 0.0997 | −0.6967 | 0.4137 | |
| 6. | 0.0000 | 0.0004 | −0.0004 | 0.0003 | 0.0003 | −0.6157 |
| Matrix elements of $D^{zx}$ | | | | | | |
| 1. | −0.7530 | | | | | |
| 2. | 0.4406 | 0.4193 | | | | |
| 3. | 0.7635 | −0.6020 | −0.2749 | | | |
| 4. | 0.2078 | 0.1000 | −0.1152 | −0.3906 | | |
| 5. | −0.1202 | 0.2303 | −0.0997 | 0.6965 | 0.4139 | |
| 6. | 0.0000 | −0.0005 | 0.0006 | −0.0005 | −0.0004 | −0.6157 |

We have also made $\mathbf{k}\cdot\mathbf{p}$ expansions around the critical point on line $Q$. Because of the lowered symmetry the interactions with other bands begin with terms of linear order. These were, however, quite small, reflecting the closeness of the critical point on line $Q$ to $L$, and the symmetry of the $\mathbf{k}\cdot\mathbf{p}$ expansion at point $L$ discussed above. We do not list these terms explicitly here. However, we can make the general statement that in the neighborhood of the critical point on line $Q$ the states are rather weakly coupled through $\mathbf{k}\cdot\mathbf{p}$ terms. The above considerations about point $L$ and the critical point on line $Q$ will play an important role in Sec. III, where they will be used to simplify the development of a Wannier function for bands 4 and 5.

The most surprising result to be derived from Table I is not that $L$ is a critical point. Due to the degeneracy of bands 4 and 5 at point $L$ the energy-band structure is fluted and cannot be quadratically expanded locally around point $L$ (and hence not be described by a second rank mass tensor). This explains the occurrence of the point $L$ as a critical point in the peak of the density of states, appearing in spite of a negative mass component along three orthogonal directions. To illustrate this point we show in Figs. 3–5 plots of contours of constant energy around point $L$ in the $(1\bar{1}0)$, (110), and (111) planes. In Figs. 3 and 4 the value of band 5 at point $L$ has been taken as the zero of energy for clarity. In Fig. 5 the value at the critical point on line $Q$ was used as the zero since we wished to show explicitly the two nearly degenerate contours representing the Van Hove $M_1$ structure. The most interesting features of the figures are the multiple narrow apex intersections at point $L$ of the degenerate cones and the hexagonal fluted behavior exhibited in the (111) plane. As can be seen, the electronic structure oscillates on the narrow scale of 30° in angle around point $L$. Clearly such a structure cannot be described by means of a second rank mass tensor. The wide spacing of the contours in these figures reflects the extreme narrowness in energy of the fifth band.

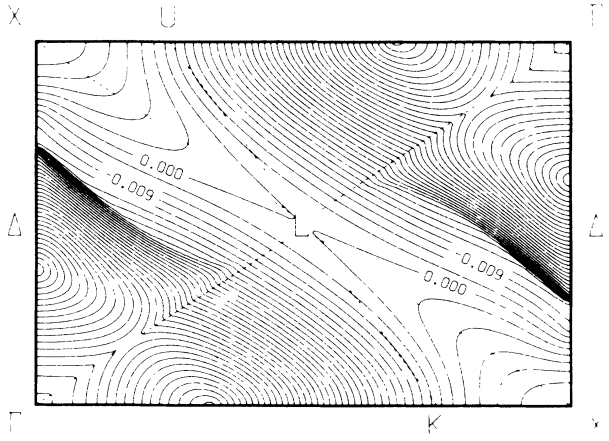


FIG. 3. Contours of constant energy of nickel in the $(1\bar{1}0)$ plane around point $L$. The energy at point $L$ has been taken as the zero of energy.

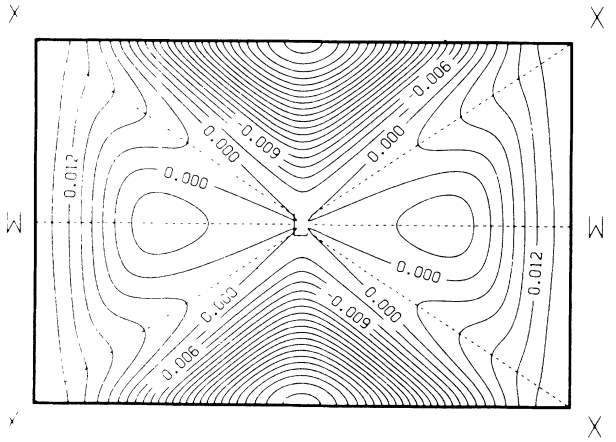


FIG. 4. Contours of constant energy of nickel in the (110) plane around point $L$. The energy at point $L$ has been taken as the zero of energy.

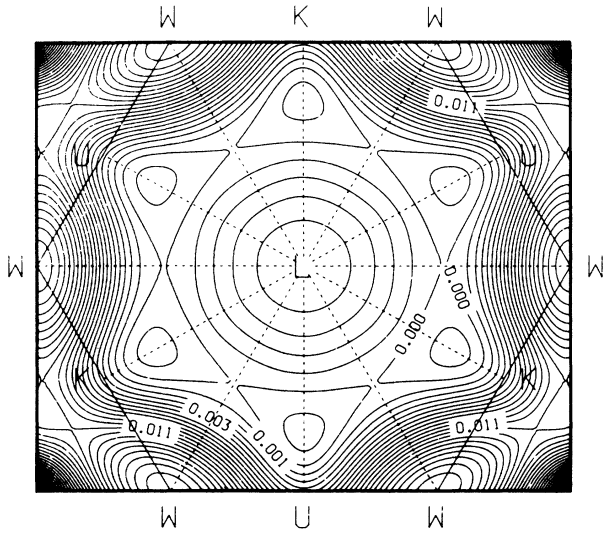


FIG. 5. Contours of constant energy of nickel in the (111) plane around point $L$. The energy at the critical point on line $Q$ has been taken as the zero of energy.

## III. NON-ATOM-CENTERED WANNIER FUNCTIONS

If we think about the wave function associated with critical points in a band, it is helpful to begin by looking at a one-dimensional system. Here there are only two types of critical points: maxima and minima, and these always occur at the high-symmetry points $\Gamma$ and $X$. In general, each band has two and only two critical points. For the one-dimensional case, the relation between the bands and the Wannier functions was completely analyzed by Kohn.[8] Kohn showed that in a one-dimensional system with reflection symmetry, the Wannier function associated with a given band will have either even or odd symmetry about either an atom-centered position or a position displaced by half a lattice constant. The point we would like to underline here is that the whole band is characterized by a Wannier function of a determined symmetry around a determined symmetry site (Wyckoff site) in the lattice. Especially the behavior of the wave functions in the region of the critical point would be strongly correlated with the appropriate type of Wannier function.

In the case of three dimensions the situation is, of course, more complicated, with multiple bands and now four types of critical points. The relation between the bands and their associated Wannier functions has been extensively studied in the literature.[9,10] Although it appears that the situation is not quite so clear-cut as in the one-dimensional case, it nevertheless remains true that in most cases a (multiple) band will be characterized by Wannier functions of a particular type—a given symmetry at a given Wyckoff site. Here we want to focus attention on the correlation between the Wannier function type and the properties of the wave functions at the critical points of the band, more specifically those critical points supplying the peak in the density of states. Now in the present case of fcc nickel there is no doubt that the single band 5 giving the dominant contribution to the peak is a $d$ band. Can we find a more compact or understandable representation for this band in terms of Wannier functions, a representation which substantially reproduces the peak in the density of states?

Our discussion of Sec. II identifies the states of band 5 in the region of the point $L$ and the line $Q$ in the BZ as generating the peak. As in the point $L$ bands 4 and 5 are degenerate, we need to consider the eigenstates of bands 4 and 5 together. Furthermore, the states of bands 4 and 5 interact only weakly with the remaining bands in this region, so that we can effectively exclude the latter from our considerations.

Having found the region of the point $L$ to be the critical one (with the line $Q$, to which we return later), we shall, in order to develop our argument, construct two bands of "pure $L$" character. The two degenerate Bloch states at point $L$,

$$\psi_L^n(\mathbf{r})=e^{i\mathbf{L}\cdot\mathbf{r}}U_L^n(\mathbf{r});\quad U_L^n(\mathbf{r}+\mathbf{R})=U_L^n(\mathbf{r});\quad n=1,2 \tag{11}$$

transform as the irreducible representation $L_3$ of $D_{3d}$ about the lattice sites $\mathbf{r}=\mathbf{R}$ and also as $L_3'$ about the interstitial Wyckoff sites $\mathbf{r}=\mathbf{R}+\tau$, where $\tau=a(\frac{1}{2},\frac{1}{2},\frac{1}{2})$. Here $D_{3d}$ is the group of the $L$ vector. In particular, the states are even or odd about the atom-centered and non-atom-centered (interstitial) sites, respectively.

The complete set of eight states in the star of the $\mathbf{k}$ vector at point $L$ is

$$\psi_{\beta_l L}^n(\mathbf{r})=e^{i\beta_l\mathbf{L}\cdot\mathbf{r}}U_L^n(\beta_l^{-1}\mathbf{r}),\quad n=1,2,\quad l=1,2,3,4 \tag{12}$$

where $\beta_l$ ($l=1,2,3,4$) with $\beta_1=E$ are four operations of $O_h$ that generate the star. We propose to model bands 4 and 5 by constructing them from suitable combinations of the Bloch states (12) with a Gaussian weighting about the $L$ points. Our ansatz will be

$$\psi_{\mathbf{k}}^m(\mathbf{r})=\sum_{n,l}c_{nl}^m\left[\left(\frac{\alpha}{\pi}\right)^{3/2}\sum_G e^{-\alpha(\mathbf{k}+\mathbf{G}-\beta_l\mathbf{L})^2}\times e^{i(\mathbf{k}+\mathbf{G}-\beta_l\mathbf{L})\cdot(\mathbf{r}-\sigma)}\right]\times\psi_{\beta_l L}^n(\mathbf{r})\quad(m=1,2) \tag{13}$$

where $\sigma$ is a vector in the unit cell, to be chosen at a Wyckoff site, and the coefficients $c_{nl}^m$ contain the phases between inequivalent $L$ points. They are determined by symmetry as we see below. The weighting factor $\alpha$ is some Gaussian parameter and the sum is over all reciprocal-lattice vectors. Note that in the limit $\alpha\to\infty$ (13) becomes simply

$$\psi_{\mathbf{k}}^m(\mathbf{r})=\sum_{n,l}\Delta(\mathbf{k}-\beta_l L)\psi_{\beta_l L}^n(\mathbf{r})c_{nl}^m\quad(m=1,2) \tag{14}$$

where $\Delta$ is the periodic $\delta$ function.

Returning to (13), we point out that the choice of $k$-dependent phase ensures periodicity in $k$ space: $\psi_{\mathbf{k}+\mathbf{G}}^m(\mathbf{r})=\psi_{\mathbf{k}}^m(\mathbf{r})$. This is necessary to obtain properly localized Wannier functions, as emphasized already by Kohn.[8,11] Wannier functions for the band (13) are con-

structed in the usual way,

$$a^m(\mathbf{r}-\mathbf{R}-\sigma)=\left[\frac{\Omega}{8\pi^3}\right]^{1/2}\int d^3k\frac{e^{-i\mathbf{k}\cdot\mathbf{R}}\psi_{\mathbf{k}}^m(\mathbf{r})}{[S^m(\mathbf{k})]^{1/2}}\quad(m=1,2) \tag{15}$$

integrated over the Brillouin zone, where $S^m(\mathbf{k})$ is the normalizing factor for $\psi_{\mathbf{k}}^m(\mathbf{r})$ and is periodic: $S^m(\mathbf{k}+\mathbf{G})=S^m(\mathbf{k})$. It is more convenient, however, to consider the localized functions obtained without the normalizing factor in (15); a simple calculation shows that they are just modulated Gaussians

$$A^m(\mathbf{r}-\mathbf{R}-\sigma)=\left[\frac{\Omega}{8\pi^3}\right]^{1/2}\exp\left[\frac{-1}{4\alpha^2}(\mathbf{r}-\mathbf{R}-\sigma)^2\right]\times\left[\sum_{n,l}c_{nl}^m\psi_{\beta_l L}^n(\mathbf{r})\right]\quad(m=1,2)\,. \tag{16}$$

The lattice of states $A^m(\mathbf{r}-\mathbf{R}-\sigma)$ is not orthogonal, of course, but they span the band (13) just as do the orthogonal Wannier functions $a^m(\mathbf{r}-\mathbf{R}-\sigma)$. The relation between lattices of Gaussian states and the corresponding lattices of Wannier functions has been discussed earlier.[12,13] From the manner of construction, the states (15) and (16) have the same symmetry around any given lattice site; since the purpose of this argument is to focus on the angular symmetry of the Wannier functions we can confine ourselves to the Gaussians (16) and ignore the incorrect radial behavior.

We see from (16) very clearly how the centering of the Gaussians depends on the choice of $k$-dependent phase in (13), as we would expect. [The centering of the Wannier functions (15) will be the same.] In view of the symmetry properties of the $\psi_{\beta_l L}^n(\mathbf{r})$ [Eqs. (12) and (13)] we shall obtain localized functions of the highest symmetry by centering them either at the atom-occupied Wyckoff sites $\sigma=0$, or at interstitial Wyckoff sites $\sigma=\tau$, both of which have full cubic symmetry $O_h$.

The $c_{nl}^m$ are then completely determined from group theory. The eight functions $\psi_{\beta_l L}^n(\mathbf{r})$ are seen from (11) and (12) to span a representation of point group $O_h$ given by the equivalent prescriptions

$$L_{3\uparrow}^{O_h}=\Gamma_{15}\oplus\Gamma_{25}\oplus\Gamma_{12}$$

(with respect to Wyckoff sites $\mathbf{r}=\mathbf{R}$) and

$$L_{3\uparrow}^{\prime O_h}=\Gamma_{15}'\oplus\Gamma_{25}'\oplus\Gamma_{12}'$$

(with respect to Wyckoff sites $\mathbf{r}=\mathbf{R}+\tau$). Since we need two bands that are degenerate at point $L$ we must project out the $\Gamma_{12}$ ($\Gamma_{12}'$) part of the representation. Then the correct combination of $L$ states in (16) is obtained by using a row projection operator on any $L$ state, say $\psi_L^1(\mathbf{r})$ of (11):

$$\sum_{n,l}c_{nl}^m\psi_{\beta_l L}^n(\mathbf{r})=P_m^{\Gamma_{12}}\psi_L^1(\mathbf{r})\equiv\psi^m(\mathbf{r})\quad(m=1,2)\,, \tag{17}$$

where

$$P_m^{\Gamma_{12}}=\tfrac{1}{48}\sum_{g\in O_h}D_{km}^{\Gamma_{12}}(g^{-1})g\,. \tag{18}$$

The operations in (18) are around $\mathbf{r}=0$ and the $D^{\Gamma_{12}}$ are matrices for $\Gamma_{12}$. The $\psi^m(\mathbf{r})$ of (17) transform as $\Gamma_{12}$ around Wyckoff sites $\mathbf{r}=\mathbf{R}$ and as $\Gamma_{12}'$ around Wyckoff sites $\mathbf{r}=\mathbf{R}+\tau$; in particular they are even for the first sites and odd for the second.

In summary, we have modeled bands 4 and 5 by two bands (13) of "pure $L$" character. In the case of choice of phase $\sigma=0$ in (13) the bands are generated by lattices of Gaussians on atom sites given [from (16) and (17)] by

$$A^m(\mathbf{r}-\mathbf{R})=\left[\frac{\Omega}{8\pi^3}\right]^{1/2}\exp\left[\frac{-1}{4\alpha^2}(\mathbf{r}-\mathbf{R})^2\right]\psi^m(\mathbf{r})\quad(m=1,2)\,, \tag{19}$$

where the $A^m$ transform as $\Gamma_{12}$ of $O_h$ around $\mathbf{r}=\mathbf{R}$. The corresponding Wannier functions (15) generating the same band will transform in the same way. On the other hand if we choose $\sigma=\tau$, the bands are generated by the non-atom- (interstitially) centered lattice:

$$A^m(\mathbf{r}-\mathbf{R}-\tau)=\left[\frac{\Omega}{8\pi^3}\right]^{1/2}\exp\left[\frac{-1}{4\alpha^2}(\mathbf{r}-\mathbf{R}-\tau)^2\right]\psi^m(\mathbf{r})\quad(m=1,2)\,, \tag{20}$$

where the $A^m$ transform as $\Gamma_{12}'$ of $O_h$ around $\mathbf{r}=\mathbf{R}+\tau$. We stress that the two choices of $\sigma$ do not lead to the same bands, as we can check from (13) [except in the limiting case (14) for $\alpha\to\infty$, where it is also easy to see that the Wannier functions are no longer localized]. We have here a situation in which we must represent the two bands as *either* of a type generated by atom-centered Wannier functions of (even) symmetry $\Gamma_{12}$ *or* of a type generated by interstitial Wannier functions of (odd) symmetry $\Gamma_{12}'$. This corresponds precisely to the situation for one dimension analyzed by Kohn and mentioned earlier.

The height and sharpness of the peak in the density of states strongly suggests that it is generated by antibonding states. This leads us to make the choice of the interstitially sited Wannier functions in our ansatz for the bands, or equivalently the modulated Gaussian functions (20). Since they transform as $\Gamma_{12}'$ they have the unusually high symmetry $h$

$$\tfrac{1}{2}(x^2-y^2)xyz,\quad\frac{1}{2\sqrt{3}}(3z^2-r^2)xyz \tag{21}$$

(relative to a site $\mathbf{R}+\tau$ as origin). To see this we have constructed functions of type (21) by projection (17) on a wave function $\Psi_L^1(\mathbf{r})$ taken from a linear augmented-plane-wave (LAPW) program of Koelling.[14] Plots in $\mathbf{r}$ space, with $\mathbf{r}=\tau$ as center of symmetry are shown in Figs. 6 and 7. Since we were most interested in the nature of the wave function in the interstitial regions, we have "un-augmented" the augmented plane waves used as the basis. This means that for plotting purposes we have approximated the functions within the atomic spheres by plane waves; the coefficients of the plane

waves were identical to their interstitial parts alone. This produces functions of correct angular symmetry (but of course improper radial structure). Contour plots of the resultant (wholly real) functions were made over $(x,y)$ planes in real space. Thirty-three contour plots were made normal to the $z$ axis and spaced every $\frac{1}{32}$ of the lattice constant. This was done so that the symmetry of the function could be examined in detail, and at every point in real space.

By means of this detailed examination, we checked that the function has indeed the novel symmetry (21) about the symmetry point $\tau$. In Figs. 6 and 7 we show a contour plot normal to $z=0.4a$. The similar plot at $z=0.6a$ is identical except for a change of sign everywhere. The plot at $z=0.5a$ does not exist because the function is everywhere zero in that plane.

Figures 6 and 7 show a multiplicity of nodal planes, normal to both the $x$ and $y$ axes, but also normal to the (110) and the (1$\bar{1}$0) planes. Indeed it becomes clear by examining the function everywhere that about the point $\tau=a(\frac{1}{2},\frac{1}{2},\frac{1}{2})$ it has indeed unusually high symmetry. [This point is not occupied by any atom in the case of Ni, but is often occupied by atoms in other crystals belonging to the $O_h^5$ ($Fm3m$) space group, i.e., crystals isomorphic to fcc Ni.]

After this somewhat detailed treatment of the $L$ functions, we carried out an identical analysis focused on the wave functions associated with the critical point on line $Q$. These functions are the ones which develop the critical structure at the bottom side of the narrow peak in the density of states of Fig. 1. There were 24 $Q$ wave functions for band 5 in the first BZ, so that in this part of our study, we decomposed a 24th-order manifold, the resulting group structure contained a multiplicity of representations—among them the same $\Gamma_{12}'$ so that the $Q$ functions contribute a symmetry at $\tau=a(\frac{1}{2},\frac{1}{2},\frac{1}{2})$ identical to the one deriving from the eight $L$ functions.

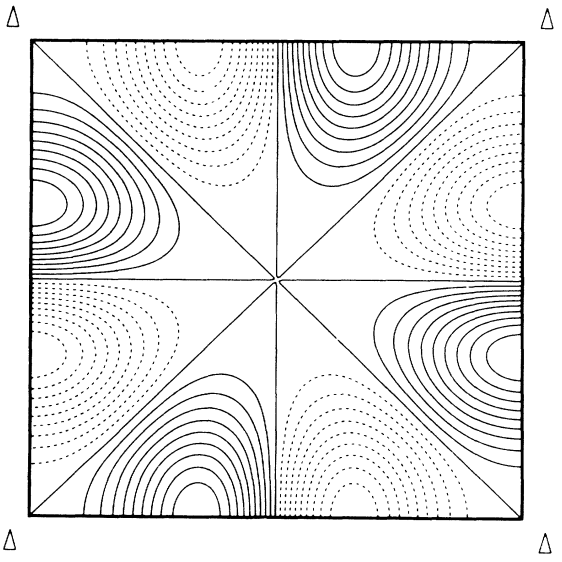


FIG. 6. The function $\frac{1}{2}xyz(x^2-y^2)$ in the $z=0.4a$ plane. The corners are a lattice parameter $a$ separated in the $x$ and $y$ directions. Note that this function has symmetry $h$ around $\frac{1}{2}a(111)$ (see text).

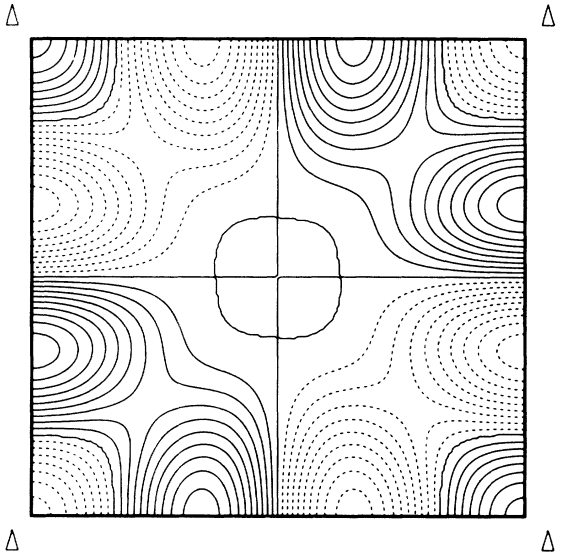


FIG. 7. The function $(1/2\sqrt{3})xyz(3z^2-r^2)$ in the $z=0.4a$ plane. The corners are a lattice parameter $a$ separated in the $x$ and $y$ directions. Note that this function has symmetry $h$ around $\frac{1}{2}a(111)$ (see text).

## IV. A SLATER-KOSTER HAMILTONIAN

In this section we address ourselves to the task of reproducing the electronic band structure to be associated with band 5 from the two special Wannier functions (20) of symmetry $h$ centered at $a(\frac{1}{2},\frac{1}{2},\frac{1}{2})$. Given the symmetry of these two special wave functions centered at $a(\frac{1}{2},\frac{1}{2},\frac{1}{2})$ discussed in Sec. III, it is natural to ask how well such states can represent the electronic band structure to be associated with band 5 and in particular the density of states in the peak region. Clearly this small sized basis will not represent the entire band structure

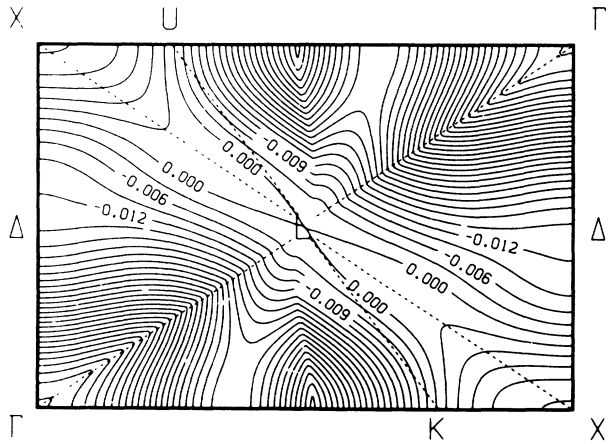


FIG. 8. Contours of constant energy of the two-band model Hamiltonian of the (1$\bar{1}$0) plane around point $L$. The energy at point $L$ has been taken as the zero of energy.

perfectly; but as discussed in Sec. III we expect the peak to be accurately reproduced. To that purpose we construct a model Hamiltonian with a Slater-Koster (SK) representation using this basis of two functions.[15] Thus we assume that we have a fcc lattice of orthonormal Wannier functions of the above type organized on the $a(\frac{1}{2},\frac{1}{2},\frac{1}{2})$ positions. We develop Bloch functions:

$$\xi_{\mathbf{k}}^{m}=\frac{1}{\sqrt{N}}\sum_{\mathbf{R}} e^{i\mathbf{k}\cdot\mathbf{R}}a^{m}(\mathbf{r}-\mathbf{R}-\tau) \tag{22}$$

where $\tau$ is $a(\frac{1}{2},\frac{1}{2},\frac{1}{2})$ and $\mathbf{R}$ is the set of fcc direct-lattice vectors. The matrix elements in the SK Hamiltonian for a general fcc vector $\mathbf{R}$ invoke at most three real SK parameters, dependent on the symmetry of $\mathbf{R}$; in Table II the three types of SK matrix elements in a fcc lattice are given.

This 2×2 SK Hamiltonian was fitted to the electronic structure of nickel. Since we wished to have an accurate fit to those points of the BZ most involved with the peak

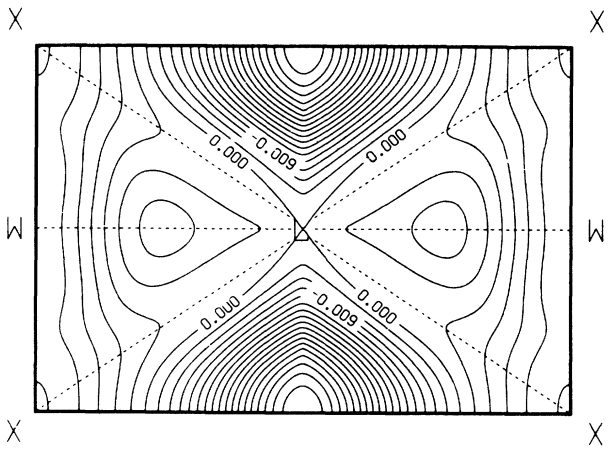


FIG. 9. Contours of constant energy of the two-band model Hamiltonian of the (110) plane around point $L$. The energy at point $L$ has been taken as the zero of energy.

TABLE II. Matrix elements of a Slater-Koster Hamiltonian for vectors $\mathbf{R}=\frac{1}{2}a(l,l,l,)$, $\mathbf{R}=\frac{1}{2}a(l,l,n)$, and $\mathbf{R}=\frac{1}{2}a(l,m,n)$. We define $\xi=\frac{1}{2}ak_x$, $\eta=\frac{1}{2}ak_y$, and $\zeta=\frac{1}{2}ak_z$. The basis states are $|1\rangle=\frac{1}{2}xyz(x^2-y^2)$ and $|2\rangle=(1/2\sqrt{3})xyz(3z^2-r^2)$.

Vector $(l,l,l)$:

$$\mathcal{H}(1,1)=8E_1\cos(l\xi)\cos(l\eta)\cos(l\zeta)$$

$$\mathcal{H}(2,2)=8E_1\cos(l\xi)\cos(l\eta)\cos(l\zeta)$$

$$\mathcal{H}(1,2)=0$$

Vector $(l,l,n)$:

$$\begin{aligned}\mathcal{H}(1,1)=&8E_1\cos(l\xi)\cos(l\eta)\cos(n\zeta)+2E_1\cos(l\zeta)[\cos(n\xi)\cos(l\eta)+\cos(l\xi)\cos(n\eta)]\\&+6E_2\cos(l\zeta)[\cos(l\xi)\cos(n\eta)+\cos(n\xi)\cos(l\eta)]\\\mathcal{H}(2,2)=&8E_2\cos(l\xi)\cos(l\eta)\cos(n\zeta)+2E_2\cos(l\zeta)[\cos(n\xi)\cos(l\eta)+\cos(l\xi)\cos(n\eta)]\\&+6E_1\cos(l\zeta)[\cos(l\xi)\cos(n\eta)+\cos(n\xi)\cos(l\eta)]\\\mathcal{H}(1,2)=&2\sqrt{3}E_1\cos(l\zeta)[\cos(n\xi)\cos(l\eta)-\cos(l\xi)\cos(n\eta)]+2\sqrt{3}E_2\cos(l\zeta)[\cos(l\xi)\cos(n\eta)-\cos(n\xi)\cos(l\eta)]\end{aligned}$$

Vector $(l,m,n)$:

$$\begin{aligned}\mathcal{H}(1,1)=&8E_1\cos(n\zeta)[\cos(l\xi)\cos(m\eta)+\cos(m\xi)\cos(l\eta)]+2E_1\cos(m\zeta)[\cos(l\xi)\cos(n\eta)+\cos(n\xi)\cos(l\eta)]\\&+2E_1\cos(l\zeta)[\cos(m\xi)\cos(n\eta)+\cos(n\xi)\cos(m\eta)]+6E_2\cos(m\zeta)[\cos(l\xi)\cos(n\eta)+\cos(n\xi)\cos(l\eta)]\\&+6E_2\cos(l\zeta)[\cos(m\xi)\cos(n\eta)+\cos(n\xi)\cos(m\eta)]-4\sqrt{3}E_3\cos(m\zeta)[\cos(l\xi)\cos(n\eta)+\cos(n\xi)\cos(l\eta)]\\&+4\sqrt{3}E_3\cos(l\zeta)[\cos(m\xi)\cos(n\eta)+\cos(n\xi)\cos(m\eta)]\\\mathcal{H}(2,2)=&6E_1\cos(m\zeta)[\cos(l\xi)\cos(n\eta)+\cos(n\xi)\cos(l\eta)]+6E_1\cos(l\zeta)[\cos(m\xi)\cos(n\eta)+\cos(n\xi)\cos(m\eta)]\\&+8E_2\cos(n\zeta)[\cos(l\xi)\cos(m\eta)+\cos(m\xi)\cos(l\eta)]+2E_2\cos(m\zeta)[\cos(l\xi)\cos(n\eta)+\cos(n\xi)\cos(l\eta)]\\&+2E_2\cos(l\zeta)[\cos(m\xi)\cos(n\eta)+\cos(n\xi)\cos(m\eta)]+4\sqrt{3}E_3\cos(m\zeta)[\cos(l\xi)\cos(n\eta)+\cos(n\xi)\cos(l\eta)]\\&-4\sqrt{3}E_3\cos(l\zeta)[\cos(m\xi)\cos(n\eta)+\cos(n\xi)\cos(m\eta)]\\\mathcal{H}(1,2)=&2\sqrt{3}E_1\cos(m\zeta)[-\cos(l\xi)\cos(n\eta)+\cos(n\xi)\cos(l\eta)]+2\sqrt{3}E_1\cos(l\zeta)[-\cos(m\xi)\cos(n\eta)+\cos(n\xi)\cos(m\eta)]\\&+2\sqrt{3}E_2\cos(m\zeta)[\cos(l\xi)\cos(n\eta)-\cos(n\xi)\cos(l\eta)]+2\sqrt{3}E_2\cos(l\zeta)[\cos(m\xi)\cos(n\eta)-\cos(n\xi)\cos(m\eta)]\\&+8E_3\cos(n\zeta)[\cos(l\xi)\cos(m\eta)-\cos(m\xi)\cos(l\eta)]+4E_3\cos(m\zeta)[\cos(l\xi)\cos(n\eta)-\cos(n\xi)\cos(l\eta)]\\&-4E_3\cos(l\zeta)[\cos(m\xi)\cos(n\eta)-\cos(n\xi)\cos(l\eta)]\end{aligned}$$

structure, we made a list of 960 random points in the BZ, whose band-5 energy fell within 3.57 mRy of the midpoint of the peak and 100 more random points within 0.5 mRy of the band-5 energy at point $L$ and the critical point on line $Q$. To force the fit to be nearly exact at point $L$ and the critical point on line $Q$, these points were included 150 and 50 times, respectively. The dispersion in energy of this set was judged as too narrow, so that 520 supplemental points were chosen along symmetry lines. The range of the supplemental points is shown in Fig. 2 as the small circles. In all, 1880 points were used in the fit. Table III lists the SK parameters derived from the fit for the different shells. Up to ten shells were included in the fit. The two energy bands of the SK Hamiltonian obtained this way are shown in Fig. 2 as the dashed lines.

As can be seen from Fig. 2, the quality of fit in the peak region near point $L$ and line $Q$ is quite good, being less than 0.3 mRy in error there, or about 6% of the peak width. Along the other symmetry lines the error is larger, but still within a few millirydbergs. The electronic structure of band 5 derived from the model Hamiltonian is compared with the corresponding original Ni structure in three planes involving point $L$ or the critical point on line $Q$ in three planes in the BZ in Figs. 8, 9, and 10. These plots show that the Hamiltonian of the non-atom-centered Wannier functions has reproduced both the structure and the topology of the peak region.

Finally we show in Fig. 11 the partial density of states for the model Hamiltonian on exactly the same scale as Fig. 1. It is clear that the peak in the density of states has been reproduced.

## V. DISCUSSION AND CONCLUSIONS

We have shown that the biggest peak in the density of states of Ni, which exists in the top end of the $d$-band region, can be viewed as arising from $h$ states of $\Gamma'_{12}$ symmetry centered at the empty Wyckoff positions $a(\frac{1}{2},\frac{1}{2},\frac{1}{2})$ in real space. The new interpretation allowed us to make a small $(2\times2)$ model Hamiltonian which fits the electronic band structure well in the region of the peak. Outside this region the electronic structure is broadly topologically correct.

TABLE III. Fit parameters of the SK Hamiltonian used in the two-band Hamiltonian (in mRy).

| Vector $(l,m,n)$ | $E_1$ | $E_2$ | $E_3$ |
|---|---|---|---|
| (0,0,0) | 90.1728 | 0 | 0 |
| (1,1,0) | −0.1300 | −4.4014 | 0 |
| (2,0,0) | −0.1625 | 0.1944 | 0 |
| (2,1,1) | −2.9050 | −1.1400 | 0 |
| (2,2,0) | 0.9575 | 1.0325 | 0 |
| (3,1,0) | −0.6725 | 0.5475 | −0.3400 |
| (2,2,2) | −1.6375 | 0 | 0 |
| (3,2,1) | 0.4925 | 0.2025 | −0.5025 |
| (4,0,0) | −0.4619 | 0.0244 | 0 |
| (3,3,0) | 0.0363 | 0.5363 | 0 |
| (4,1,1) | 0.6050 | 0.2200 | 0 |

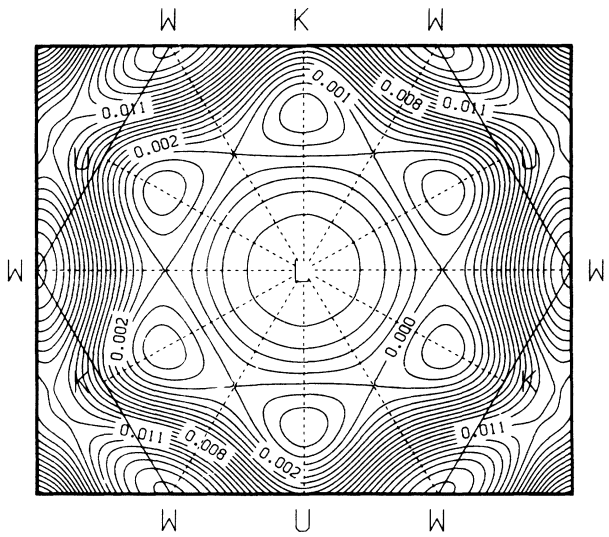


FIG. 10. Contours of constant energy of the two-band model Hamiltonian (111) plane around point $L$. The energy at the critical point on line $Q$ has been taken as the zero of energy.

The novel symmetry Wannier function we have developed around $a(\frac{1}{2},\frac{1}{2},\frac{1}{2})$ is perhaps the maximally antibonding interstitial state we could have constructed. That such a state fits the electronic structure of the peak so well is strongly suggestive that *this* state generates the abnormally tall peak in Ni. Evidently the fcc lattice combines with $d$-like orbitals to produce this special type of antibonding state. Another system in which a simple but realistic band structure based on non-atom-centered Wannier functions has been studied is the "two-dimensional" metal $Hg_3AsF_6$.[16]

How general is this notion? It is clear, as we men-

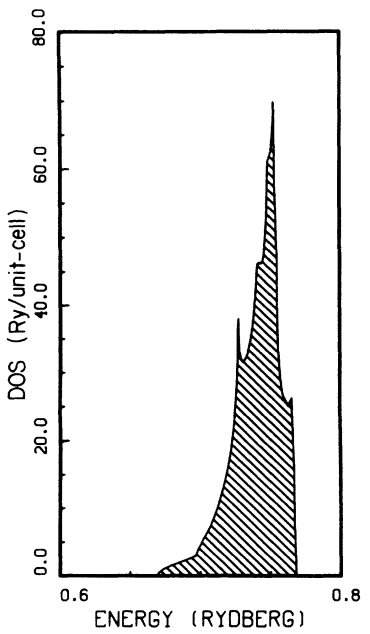


FIG. 11. Density of states of the model Hamiltonian for the band designed to fit the original band 5.

tioned in the Introduction that there are many different crystal structures related to the fcc structure in the positions of the atoms. Therefore we do not think that the special relationship of a maximally antibonding Wannier function to peaks in the density of states is either limited or rare. Both the $A15$ and perovskite structures come to mind and are suggestive of further study.

We conclude that we have isolated a reason for the extraordinarily high peak of the density of states of Ni. There is a direct relationship between the highest peaks in the density of states and Hamiltonians constructed from Wannier functions of special symmetry centered at non-atom-centered positions.

## ACKNOWLEDGMENTS

Part of this work was supported by the U.S. Department of Energy. Most of this work was performed while one of us (G.H.O.D.) was employed by the Center for Materials Science. One of us (M.H.B.) is grateful to the Center for Materials Science for support and hospitality during several visits.

[1]L. Van Hove, Phys. Rev. **89**, 1189 (1953).
[2]J. C. Phillips, Phys. Rev. **104**, 1263 (1956).
[3]The band structure was generated by means of the augmented-spherical wave (ASW) method; see A. R. Williams, J. Kübler, and C. D. Gelatt, Phys. Rev. B **19**, 1990 (1979). In the present work the spin-down band structure is used.
[4]W. Joss and G. W. Crabtree, Phys. Rev. B **30**, 5646 (1984), and references therein; D. H. Dye, J. B. Ketterson, and G. W. Crabtree, J. Low Temp. Phys. **30**, 813 (1978), and references therein.
[5]P. O. Löwdin, J. Chem. Phys. **18**, 365 (1950).
[6]See the discussion in J. Callaway, *Quantum Theory of Solids* (Academic, New York, 1974), Pt. A, p. 246.
[7]E. I. Zornberg, Phys. Rev. B **1**, 244 (1970).
[8]W. Kohn, Phys. Rev. **115**, 809 (1959).
[9]J. des Cloizeaux, Phys. Rev. **129**, 554 (1963); **135**, A685, A689 (1964).
[10]J. Zak, Phys. Rev. Lett. **45**, 1025 (1980); Phys. Rev. B **23**, 2824 (1981); **25**, 1344 (1982); **26**, 3010 (1982).
[11]W. Kohn, Phys. Rev. B **7**, 4388 (1973).
[12]G. H. Wannier, J. Math. Phys. **19**, 131 (1978).
[13]F. M. Mueller, M. H. Boon, M. Tegze, and F. van der Woude, J. Phys. C **19**, 749 (1986).
[14]We wish to thank D. D. Koelling for providing us with a copy of his program.
[15]J. C. Slater and G. P. Koster, Phys. Rev. **94**, 1498 (1954), called SK in the text.
[16]J. J. M. Buiting, M. Weger, and F. M. Mueller, J. Phys. F **14**, 2343 (1984).